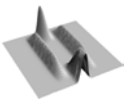

4.5 Mach-Zehnder Interferometer (MZI)

Interferometry has devoted much interest in integrated optics due to the many fields where it can be applied ranging from chemical sensing **[16]** to multiplexing **[2]**. Between the different configurations that lead to interferometric patterns, Mach-Zehnder is the most widely structure employed. This is mainly due to the fact that it generally shows very high sensitivity (when acting as a sensor), high contrast and easiness on its design. Nevertheless, up to date MZI has only been applied to research or prototype sensor applications due to several inherent problems **[17]** which will be briefly highlighted.

As it was described in chapter 2, a small variation of the optical path in one of the branches causes to have interferometric patterns at the device output, as they are schematically shown in fig. 4.28. This type of interference pattern lead to ambiguity when determining the phase change since two values with a $\Omega 2\pi$ phase variation (shown in fig. 4.28 as ●) have the same intensity value. Moreover, the MZI sensitivity, which can be associated to the slope of the fringe pattern, clearly decreases as the intensity approaches to its extreme values. At these points, phase changes are not accurately measured, causing a sensitivity fading. In addition, there exists some extrinsic disturbing factors, as could be temperature measurement fluctuations and, as discussed in the previous section, technological imperfections.

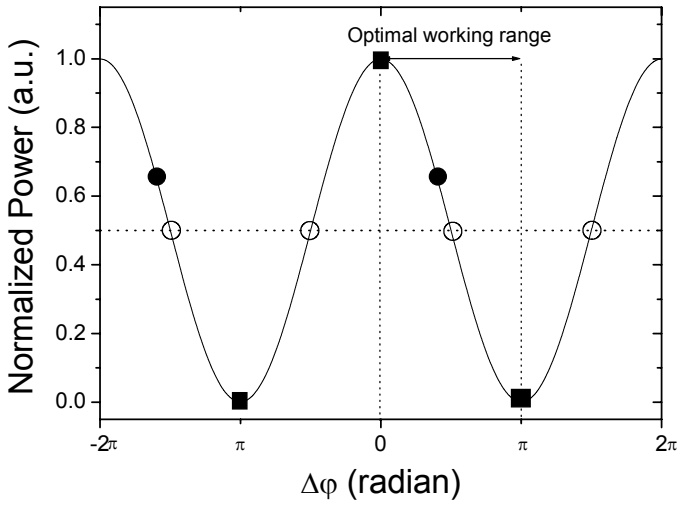

Fig 4.28. Schematic plot of the normalized intensity measured in a MZI versus the phase difference $\Delta\varphi$, showing the fringe pattern, the inherent interferometer problems (■ Sensitivity fading; ● Fringe order ambiguity) together with the optimum initial position in quadrature (◌) and the optimum working range.

A possible solution in order to solve the intrinsic MZI problems would be to adjust the phase range to a half fringe. This however will result in a decrease of the resolution and the detection limit. Alternative configurations are based on an externally-driven phase modulation **[18]**, **[19]** applied to one or both sensing arms that provides with a reference from which total phase variation can be obtained without ambiguity.

As far as geometry is concerned, several modifications of the basic structure have been proposed in order to enhance sensing properties and minimize attenuation. It has previously been studied that straight Y-junctions have relatively high losses for tilt angles above 1º. An alternative approach could consist on changing the output Y-junction by a 3x3 directional coupler **[10]**. Thus, the interference patterns obtained would be phase shifted with respect to each other by nominal $2\pi/3$ rads. By this way, it is assured that at least one out of the three output waveguides show a sensitive response to phase variations. Moreover, the sum of all the three outputs remains constant, being able to be used as a reference with much higher signal-to-noise ratio (SNR).

As a first step, we have implemented a single 2x1 directional coupler that couples light coming from both branches of the MZI interferometer, which we have labeled as DC-MZI. Simulations shown in table 4.5 were done considering 5μm width 2μm rib ARROW-A waveguides distanced 2μm. After a distance equal to the coupling length (3550μm), light was 3dB split on each arm. A small perturbation was applied on the 5mm sensing zone, located on one branch. As can be seen in table 4.5, if the phase difference between both branches is an even multiplier of π, constructive interference occurs and power transference is maximum. On the contrary, odd π phase difference causes a superposition of two evanescent tails with identical magnitude but different in sign, that inhibits light coupling to the outer waveguide.

Thus, power at the output waveguide depends on the phase difference between light propagating by both MZI branches, The transition from complete coupled to uncoupled waveguides can be observed in fig. 4.29. Although an interference pattern is obtained, it has to be noted that this is not directly due to the modal superposition, as it was the case in the Y-junction, but to a evanescent field overlap that allows or prevents from modal coupling at the output waveguide.

	$\Delta\varphi = 2\Omega\,\pi$	$\Delta\varphi = (2\Omega+1)\,\pi$
Phase	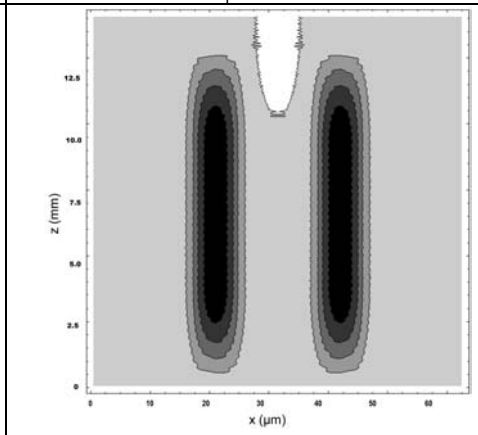	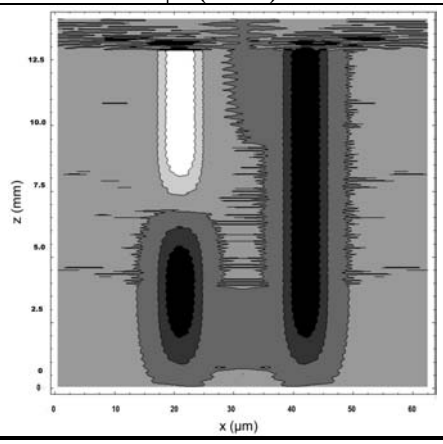
	$\Delta\varphi = 2\Omega\,\pi$	$\Delta\varphi = (2\Omega+1)\,\pi$
Intensity	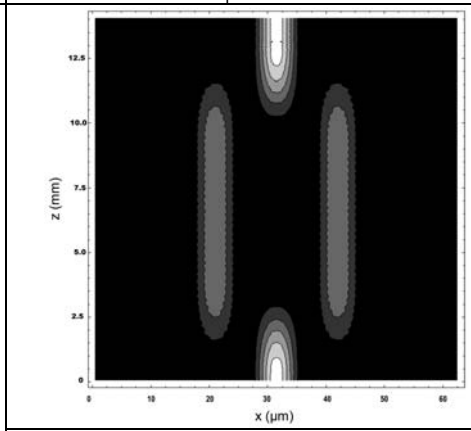	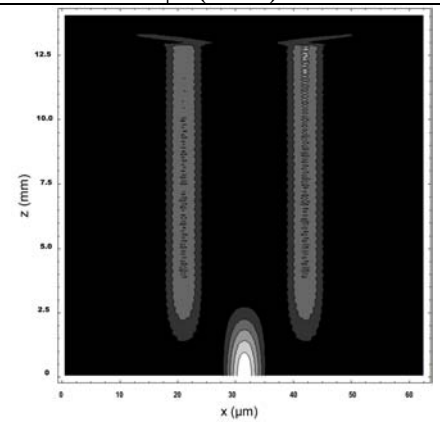
	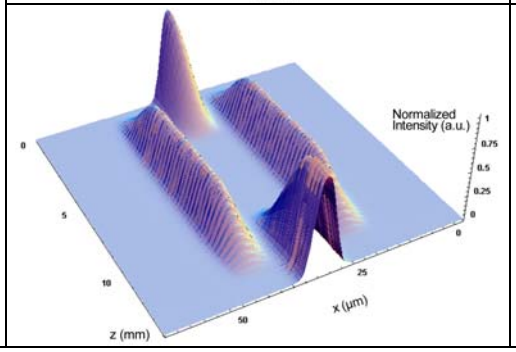	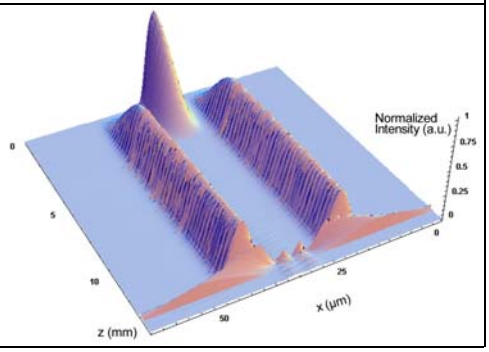

Table. 4.5. Phase and intensity at the output of a MZI with directional coupler inputs and outputs.

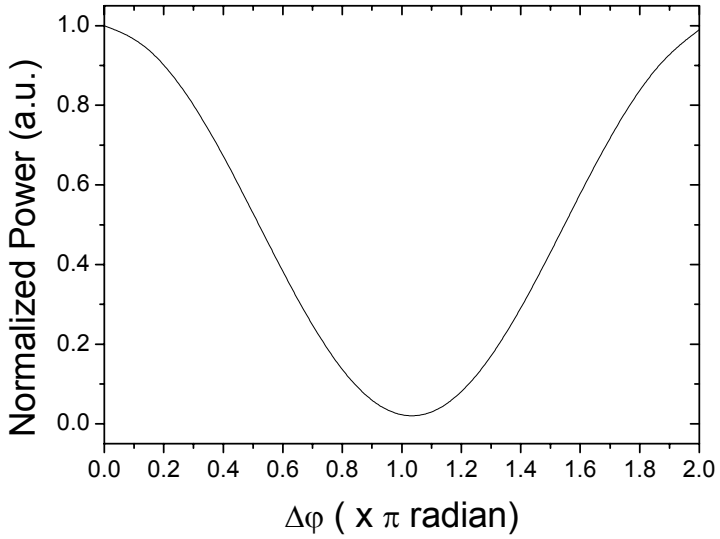

Fig 4.29. Normalized power coupled in the output waveguide as a function of the phase difference between the modes propagating on both MZI branches.

From the basis of the previously designed 3dB splitters, a huge variety of interferometers could be designed so as to provide with optimum contrast. Actually, apart from the well known Y-Y (Y-junction in, Y-junction out) structure, MMI devices have already been applied to MZI design, obtaining the so-called generalized Mach-Zehnder Interferometers, used in telecommunication applications **[20]** and 3x3 directional couplers have proved its viability for overcome fading. However, low attention has been paid to the input Y-junction, which perhaps has a major importance, since it is the responsible of the appropriate 3dB splitting. Moreover, excessive losses in the 3dB splitting region would not cause malfunctions on the device properties, but the SNR value will decrease, causing the measure to be noisier and inaccurate. In addition to the previously studied DC-MZI, two additional novel configurations have been designed, which we have labeled as U-Y and U-DC. Both take advantage from the previously studied properties of the parabolic 3dB splitter. Evolution of the intensity as a function of the propagation distance is shown in fig. 4.30. Light has been injected in a 40-μm width multimode waveguide directly connected to a parabolic 3dB splitter. It can be observed how the parabolic splitter progressively changes its modal properties, from highly multimode to single mode. After 3800μm, light is injected to a 4μm single mode waveguide on each arm. In order to analyze the goodness of the configuration designed, we have considered $\Delta\varphi=0$ and thus, constructive interference should be produced at the

MZI output. Waveguides are recombined via a standard Y-junction with 5º tilt (fig. 4.30a). In the case presented in fig. 4.30b, light waveguides are firstly tilted exactly in the same way as they were in case (4.30a). When the separation between them is 8µm, a 4µm-output waveguide is equidistantly placed between them, forming a 2x1 directional coupler configuration.

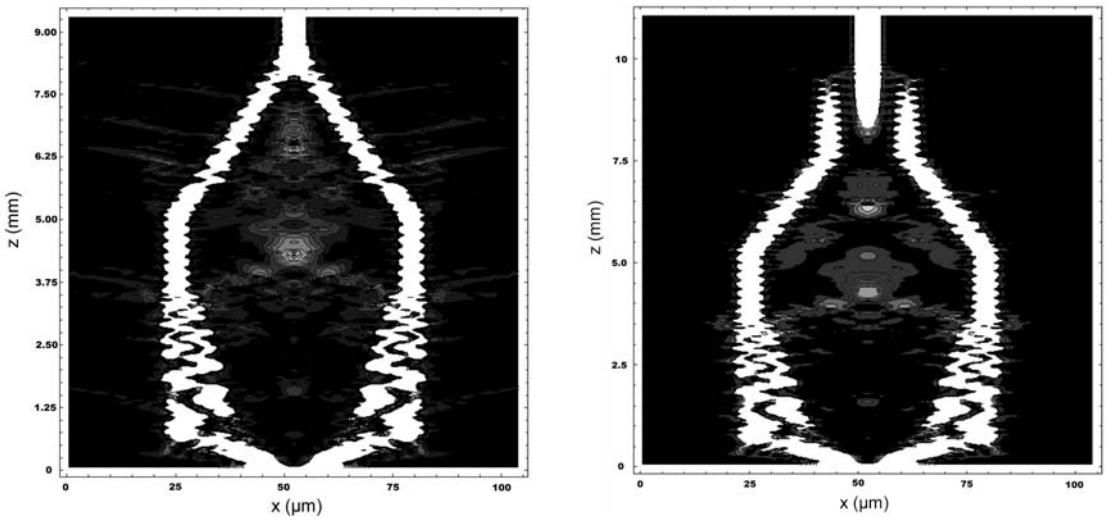

Fig 4.30. Light intensity propagation in the proposed MZI devices: a) U-Y configuration. b) U-DC configuration.

Several advantages can be observed in these configurations as compared to standard MZI configurations. Firstly, dimensions have been significantly reduced. Actually, parabolic splitters could be done even smaller in size while keeping losses below the values obtained for straight Y-junctions. It has also been observed that parabolic 3dB structures fulfill both the optical and technological requirements, having minimum sizes of 2µm while providing with an excellent splitting. Thus, SNR significantly increases, causing the MZI to be more sensitive when applied to sensors field.

For sensing purposes, integrated device should have high sensitivity, that is, the sensor response to external changes is expected to be as high as possible. This sensitivity is a function of the strength and distribution of the evanescent field in the outer medium **[21]**. Two different sensitivities can be distinguished depending on how the refractive index changes are produced in the outer medium: homogeneous sensing is

obtained when this change is homogeneously distributed in the external media. It is related to the power of the guided mode transported in the cover medium (Fig. 4.31a). On the other hand, if there is an adsorption of molecules from a gaseous or liquid sample on the waveguide surface, the sensing process is known as surface sensing, whose sensitivity is related to the squared field magnitude at the core-cover interface (Fig. 4.31b).

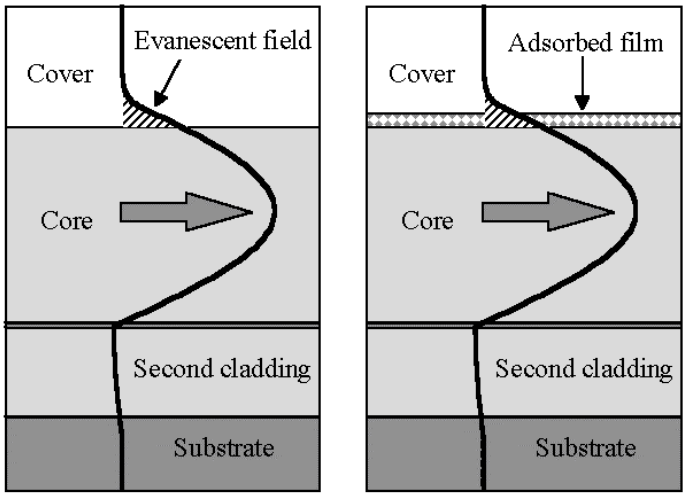

Fig 4.31. a) Homogeneous sensing. b) Surface sensing, after **[22]**.

As it has been analyzed in **[23]**, homogeneous sensitivity increases as the core thickness diminishes due to a less confinement factor within the core, which implies a larger evanescent field propagating through the cover medium. Moreover, this sensitivity is also dependent on the refractive index of the core, since a larger value implies a decrease in the penetration depth of the evanescent field and, therefore a reduction of the homogenous sensitivity.

The interaction between a receptor molecule adsorbed on the waveguide surface and an analyte can be understood as a mass change in the molecular adlayer and, therefore, as a variation in its refractive index. Surface sensitivity is then related to the value of the evanescent field at the waveguide surface. Assuming that the adsorbed molecules form a homogeneous adlayer of thickness d_{mol} and refractive index n_{mol}, sensitivity is evaluated as the rate of change of the effective refractive index of the guided mode, with respect to d_{mol}. It is clear that when the core thickness increases,

surface sensitivity decreases due to a higher confinement of the mode within the core layer **[23]**.

Both types of sensitivity can be increased by overcoating the surface of the sensor with a very thin higher refractive index layer **[24]**. As the overlay thickness increases, the field profile is progressively distorted in such a way that the field penetration into the cover medium is higher compared to the uncoated ARROW enhancing its sensitivity (Fig. 4.32). If a certain d_{ov} is reached (which for ARROW-A structure has a value of 40nm for TE modes) the ARROW fundamental mode is transformed to the lowest order mode of the overlay, that behaves as a TIR waveguide. Thus, it is essential for sensing applications that d_{ov} remains below 40 nm. Moreover, it has to be taken into account that the distortion of the ARROW fundamental mode implies a decrease in the coupling efficiency between the waveguide and the optical fiber.

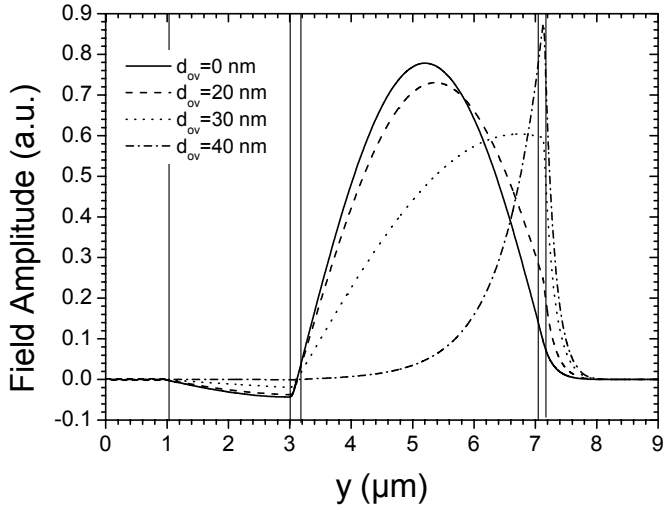

Fig 4.32. Transformation of the field profile for the TE_0 mode in an ARROW structure as the overlay thickness increases.

Thus, the configuration of the standard MZI has been modified so as to optimize the 3dB split in each waveguide while achieving minor losses in a more compact structure, by ways of U-junctions and directional couplers. Moreover, it has been briefly exposed the possibility of enhancing the sensitivity by having a thin overlay that causes the field profile to be modified, causing an increase of its evanescent field. Results of this section are summarized in table 4.6.

	Splitting	Junction	Total length (mm)	Maximum d_{ov} value (nm)	Homogeneous Sensitivity	Surface Sensitivity (10^{-4} nm^{-1})
MZI-I	DC-	DC-	15	35	0.03	0.45
MZI-II	U-	Y-	10			
MZI-III	U-	DC-	12			

Table 4.6: Different proposals for MZI interferometers based on ARROW-A structures. Sensitivity values have been extracted from **[16]**.

4.6 Absorption sensor

In chapter 2, the basic configuration of an absorption sensor was highlighted. Its operation principle is based on the variation of the imaginary part of the propagation constant for a given membrane as a function of the analyte concentration to be detected. The basis of an optochemical sensor is the detection of a certain analyte through a specific receptor molecule that causes a significant change in the system conditions (for instance, a variation of its absorption coefficient at the working wavelength). In our case, the objective was the detection of potassium ions. A two-step detection mechanism has been employed. Firstly, the membrane has a compound, called ionophore that is able to react with the analyte. This reaction has, as a consequence, the structural modification of another compound, called cromophore, which causes modifications on the membrane optical properties. In other words, when the analyte reacts with the ionophore, a change is produced in the proximity of the cromophore that causes a modification of the membrane absorption bands.

In order to obtain a feasible optochemical sensor, the membrane must fulfill strong requirements: **1. Specificity:** the ionophore must react only with the analyte to be detected. Moreover, reactions that take place during its detection must be reversible. Finally, the modification of the cromophore absorbance spectra has to be produced at the working wavelength. **2. Maximum sensitivity:** both ionophore and cromophore are included in a polymer matrix that allows appropriate membrane positioning. This polymer matrix should not react neither with the analyte nor change its properties as a function of the wavelength. It should also allow analyte in-diffusion. Thus, its thickness

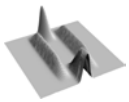

becomes essential, since the detection principle is diffusion-limited. Thick membranes would require excessively long time for the analytes to reach the ionophores placed at the region between the waveguides (which are the responsible of the optochemical detection), moreover, diffraction in the y axis would also occur, causing an increase of the losses. On the other hand, for membranes thinner than the waveguides (<4μm) sensitivity would be partially lost since light would not completely interact with the membrane. Moreover, it would find an interface between two different media that would increase the membrane insertion losses. As far as membrane total length is concerned, sensitivity increases as the length increases. However, as it was described in chapter 2, due to diffraction, the electromagnetic field progressively broadens in the free-space region. Thus, even if the output waveguide is wider than the input one, an agreement must be reached between the sensitivity and the total length.

Concretely, in order to compensate the diffraction effects, input and output waveguides were designed to be 20μm and 60μm width, respectively. The membrane zone was 500μm in length **[1]**. In according to the section 2.3.1.1, this configuration has the light divergence effects fully compensated in the x direction, being its losses only due to diffraction in the y-axis (vertical). In fig. 4.33a, it can be observed how light launched from the input waveguide is collected by the output waveguide after crossing the free space region, where it broadens. During this simulation, no absorption was considered to take place. However, the same study can be done considering a membrane with a complex refractive given by (n+iκ), where n=1.46 and κ, called the extinction coefficient, is related to the absorption coefficient by:

$$\alpha = \frac{4\pi\kappa}{\lambda} \tag{4.1}$$

Results of the optochemical sensor as a function of the absorption coefficient at a working wavelength of 633nm are presented in fig. 4.33b. Attenuation as a function of κ has the expected exponential-decaying shape, following the form $e^{-2\alpha z}$. Thence, for a fixed device length, losses have a linear dependence on the absorption coefficient.

As a conclusion of this subsection, the basic configuration of the proposed absorption sensor is given in table 4.7. It can be observed that thanks to the increase of the output waveguide, light losses due to beam divergence in the x direction are

neglectable. Nevertheless, this is no so at the *y* axis, where, since the input and output have in this direction the same size, high losses are unavoidable. Thus, although it means lower sensitivity, distance between waveguide must be as minimum as possible, in order to have the highest SNR available.

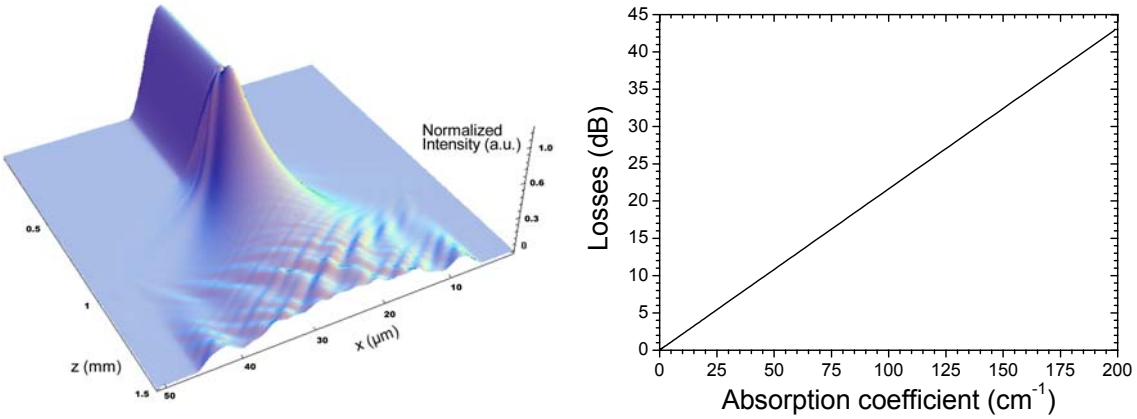

Fig 4.33. a) Normalized intensity propagation in an optochemical absorbance sensor. b) Total losses in the absorbance sensor as a function of the membrane absorption coefficient.

	Input waveguide width (μm)	Output Waveguide width (μm)	Total length (μm)	Losses in y axis (dB)	Losses in x axis (dB)
ABS-I	20	60	500	12	0.02

Table 4.7: Parameters of the proposed ARROW-A based absorbance sensor configuration.

4.7 Diaphragm Uniaxial Optical Accelerometer

In chapter 2, the basic configuration of a diaphragm-based optical accelerometer was presented. From the optical point of view its configuration is identical as compared to the optical absorption sensor: an input waveguide injects light into a free-space region that, after a given distance, is collected again by a wider output waveguide. However, instead of a analyte-sensitive membrane, a variable diaphragm has been placed between the waveguides. In order to fully characterize this device, both optical and mechanical simulations have to be done. Firstly, losses as a function of the diaphragm position will be studied so as to determine the span where a linear region is obtained. In turn, this result will be essential on designing the mechanical parts of the

accelerometer, since the seismic mass movement is, for a given acceleration, strongly dependent on the geometry of the beams.

Optical simulations were done considering a vertical cut along the y-z plane, as shown in fig 4.34. A standard 4-µm ARROW-A structure was used, being the separation between them of 50µm. The silicon diaphragm was 30µm width, in according to the preliminary results obtained in chapter 2.

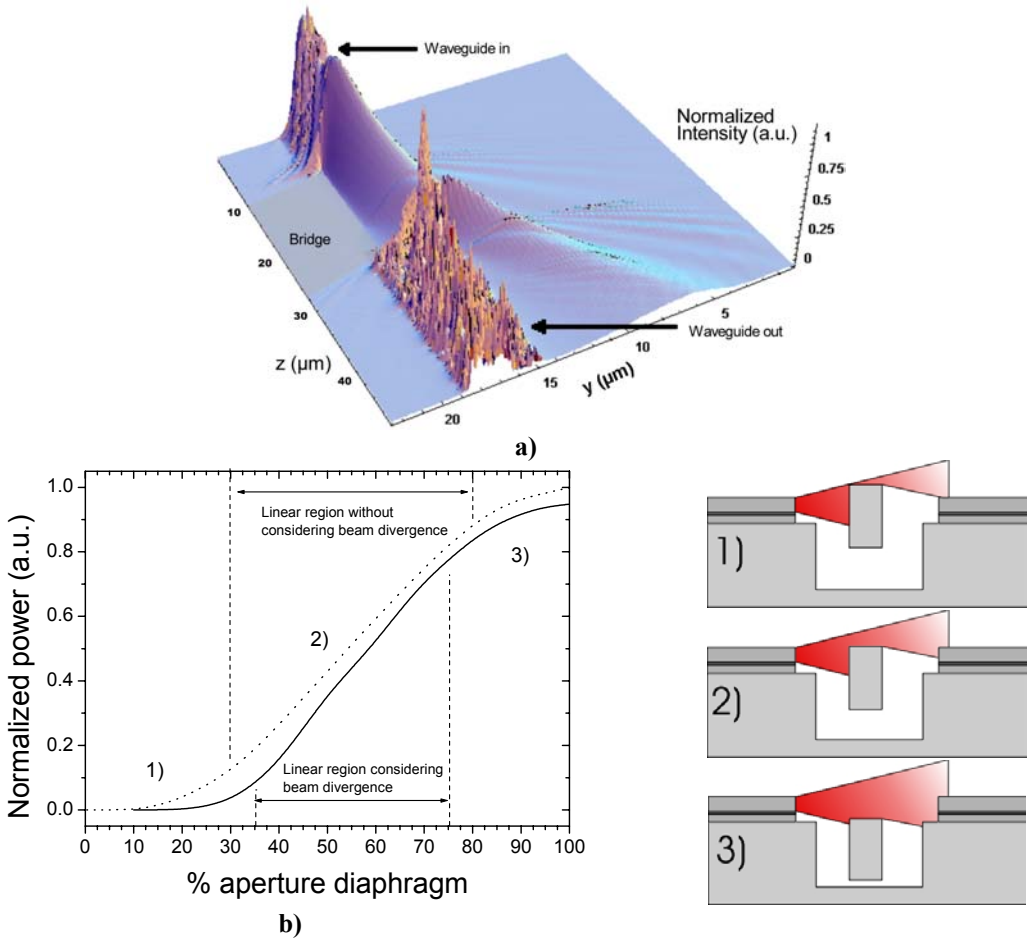

Fig 4.34. a) Normalized intensity propagation in an optical accelerometer with its diaphragm opened 45%. b) Normalized power as a function of the diaphragm aperture with (solid line) and without (dashed line) considering beam broadening.

As can be observed in fig 4.34b, the power transmitted to the second waveguide is low for apertures below 30-35%. This could be associated to the fact, that, since the power limiter is nearly covering the waveguide cross-section, light injection is produced near the upper interface, causing the excitation of higher order modes that, due to the ARROW guiding properties, are unguided through the output waveguide.